Numerical Analysis of Helicopter BVI Noise in Turning Flight

By
Choongmo Yang, Takashi Aoyama, Hirokazu Ishii and Yoshinori Okuno
Japan Aerospace Exploration Agency (JAXA)
7-44-1, Jindaijihigashi-machi, Chofu, Tokyo 182-8522, Japan

ABSTRACT

Blade-Vortex Interaction (BVI) is known to be one of the most annoying sources of helicopter noise. In order to obtain acoustic waveforms of BVI noise, a series of flight tests was conducted by JAXA's MuPAL-ε research helicopter using a microphone mounted on its nose boom. The measured acoustic data of the flight tests shows apparently stronger BVI noise in turning flight than in straight flight at the same airspeed and vertical speed. From the flight conditions, two cases, a straight descent and a descending turn, are chosen to compare the noise pattern with CFD computation and to understand the BVI noise characteristics during coordinate turns. Trim data obtained through a flight simulation code are given to CFD computation for two cases. CFD simulation successfully reproduces the tendency of increasing BVI noise due to the turning maneuver at least for the present flight conditions.

1. INTRODUCTION

Helicopters radiate an excessive slapping noise called Blade-Vortex Interaction (BVI) noise during approach, and this is known as one of the most annoying helicopter noises during terminal operations. BVI noise is generated by impulsive pressure fluctuations on main rotor blades induced by tip vortices shed by the preceding blades. Since the distance between the blades and vortices become small at "moderate" descent angles, strong BVI noise is radiated during conventional approach flight conditions.

Many researches including experimental and computational activities[1-4] have been conducted to understand the physics of BVI noise and to reduce the BVI noise. However, most of the researches have been restricted to steady flight conditions in order to simplify the phenomena. If considering real-world helicopter maneuvering in complex motion including unsteady or transient effect as well as pitching, rolling and yawing motions, the helicopter noise becomes much more complicated. In transient flight conditions, the unsteady blade air-loads and blade motions are known to produce dramatic increase of radiated noise[5]. During this transient motion, wakes and tip vortices can be fully unsteady and 3-dimensionally-aperiodic, which also give rise to significant increase of interaction noise compared to the noise in steady flight. Because of the complexity of the problems, not so many researches have been addressed on the noise prediction of a maneuvering rotorcraft. Brentner et al.[6] have conducted computational analysis using free-vortex wake model and acoustic code to predict the unsteady loading during simple maneuvers, such as turning and descending flight compared to level flight. Ananthan et al. [7] predicted transient aerodynamics of rotor wake in response to time-dependent blade pitch inputs. Chen et al. [8, 9] also examined three types of flight maneuvers, namely arrested descent, turns, and roll-reversal maneuvers using rotorcraft aero-acoustics prediction model. Munsky et al. [10] analyzed BVI noise with flight path or attitude modification in low-speed descent. Perez et al. [11] extended the cases to other types of maneuvers using aerodynamic/acoustic computation chain for BVI noise prediction. Yang et al.[12] analyzed the noise generated from a maneuvering rotorcraft with modified governing equations, which are derived for maneuvering helicopter analysis using coordinate transformation from inertial (fixed) coordinate into non-inertial moving (translating) coordinate, then two simple maneuvering cases were calculated.

The Japan Aerospace Exploration Agency (JAXA) developed MuPAL-ε research helicopter, and has been carrying out various acoustic flight tests[13] to obtain basic noise data for several maneuvering conditions. The obtained acoustic pressure shows that significant large BVI noise could occur during descending turns compared to the normal BVI noise, which is the same pattern as analysis results[6-12] of turning flight. For the better understanding of the reason of these strong BVI noise pattern for turning flight, it grows necessary to solve the ideal turning flight condition using CFD to check whether the same pattern appears in simulation or not.

JAXA has also been developing its own CFD code[14] to solve full helicopter simulation using accurate flow solver and acoustic solver. Some previous researches have shown its ability to capture the distinct peak of BVI noise for several problems including active control analysis[15,16]. Also the code expanded its ability to solve the flow-field including tail-rotor and fuselage configuration including interaction noise analysis[17].

The objective of the present paper is to compare computational results with measured data of flight test by MuPAL-ε research helicopter to understand the BVI noise characteristics during coordinate turns. Special focus will be brought into the phenomena of sudden increase of BVI noise according to the specified bank angles and vertical speed, where the abnormal increase of BVI noise happened at MuPAL-ε flight test.

2. FLIGHT TEST

2.1 JAXA's Experiment

JAXA is carrying out a research program[18] of three dimensional curved flight paths to enhance the capacity and efficiency of small regional airports and reduce the noise

impact on surrounding communities. JAXA's research helicopter, MuPAL-ε, is a twin turbo-shaft 4500kg machine with a four-bladed main rotor. Table 1 shows its key specifications of MuPAL-ε. The aircraft is equipped with an experiment support system comprising various sensors as described Ref. 19.

Table 1: MuPAL-ε key specifications.

Aircraft Type	Mitsubishi MH2000A	
Max. T/O Mass	4500kg	
Max. Horizontal Speed	140kt	
Engines	2×876shp MG5-110	
Rotors	Main	Tail
Radius	6.1 m	0.55 m
Chord	0.40 m	0.087 m
No. of Blades	4	10
Rotational Speed	317 rpm	3500 rpm
Direction of rotation	CCW	

2.2 Acoustic Apparatus

Figure 1 shows an overview of the nose microphone of the MuPAL-ε research helicopter. In order to minimize installation cost, the nose microphone was attached to a nose boom which originally carried air data sensors. A nose cone was used to reduce wind noise, and the gaps and steps between the microphone and the adapter were wrapped with adhesive-backed aluminum tape to minimize aerodynamically induced noise. The measured sound pressure was recorded at a sampling frequency of 48kHz by a DAT (Digital Audio Tape) recorder mounted on a rack in the cabin. Furthermore, a microphone held by the operator in the cabin was used to measure cabin noise at the point between the pilot seat headrests. The detail of acoustic apparatus is described in Ref. 19.

The measured noise includes noise from the engines and gearbox as well as noise from the main rotor. A main rotor one-per-rev trigger is necessary to extract only the noise from the main rotor, and so a sensor consisting of a laser pick-up and a reflector was installed on the swash plate. The one-per-rev trigger signal was recorded by the DAT recorder simultaneously with acoustic data.

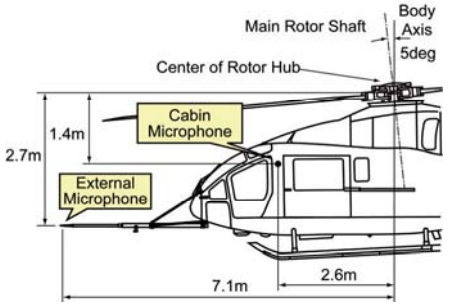

Fig.1: Diagram of Nose microphone.

2.3 Flight Conditions

The flight conditions for noise measurement were established as combinations of indicated airspeed, vertical speed, and bank angle. Level, climbing, and descending flights were flown at airspeeds of 50-140kt, and vertical speeds of between 500fpm (climb) and -1500fpm (descent). The corresponding flight path angles ranged from -18 to 6 degrees. Level and descending turns were flown to obtain basic data for the development of noise abatement approaches using curved flight paths. Airspeed and vertical speed were the same as for straight flight; that is, flight conditions were combinations of airspeeds of 50, 70, and 100kt, descent rates of 0, 600, and 1000fpm, and bank angles of ±15 and ±30 degrees. Cases with different vertical speeds were flown successively at altitudes of 1000–5000ft for the efficient tests, and many cases were conducted in a single flight, during which the mass of the helicopter varied by up to the maximum of 460kg, which corresponds to about 10 percent of the maximum take-off mass.

2.4 Measured Acoustic Data

BVI noise is known to contain about the 10–50th harmonics of the blade-passing frequency of the main rotor.[20,21] Since the blade-passing frequency of MuPAL-ε is 21Hz, the aircraft's BVI noise contains frequencies between 200Hz and 1kHz. In order to extract the BVI noise, a combination of a low-pass and a high-pass filter was applied to the measured data. The low-pass filter was a 5th-order Butterworth filter with cut-off frequency of 1200Hz, while the high-pass filter was a 3rd-order Butterworth filter with cut-off frequency of 180Hz. In order to enable zero-phase distortion, each filter was applied in the backward direction after being applied in the forward direction. Figure 2 compares the analysis for measured data. The SPL spectrum of the filtered data in the middle row shows that the filters have passed frequency components between 200Hz–1kHz, and remaining components have been effectively attenuated. The time history of filtered sound pressure shows clearly the waveforms of BVI noise, so the filtering is appropriate for examining the changes of the waveforms according to flight condition.

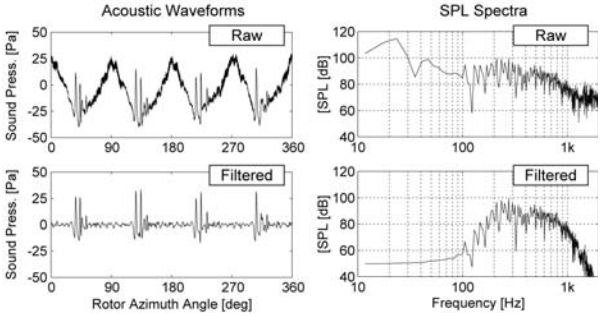

Fig.2: Comparison of data analysis for measured data

3. NUMERICAL SIMULATION

3.1 Overlapped Grid Method

A moving overlapped grid system with three different types of grids (blade grid, inner and outer background grids) shown in Fig. 3 is used. The inner background grid is placed around the rotor disk. The outer background grid covers the whole computation region with a sparse grid density. The flow data are exchanged between the inner and outer background grids, and between the blade grid and the inner-background grid. The body-fitted blade grid in O-H topology moves along with the blade motion including rotation, flapping, feathering, and lagging.

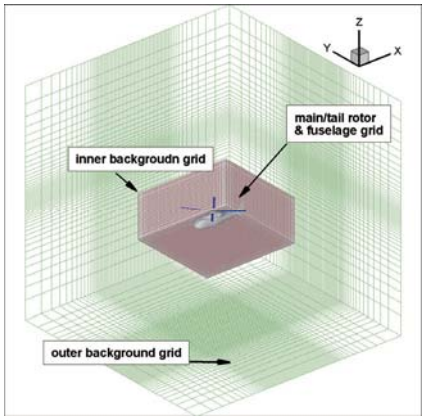

Fig.3: Overlapped grid system

Table 2: Specification of grid system.

Inner background grid	(X×Y×Z) 290×270×180 = 14,094,000
Outer background grid	(X×Y×Z) 83×79×49 = 321,293
Blade grid	(chord×normal×span) × blade (125×25×95) × 4 = 1,187,500
fuselage	171×21×150 = 538,650
Total	~16,100,000 points
Inner background spacing	0.08c (=0.0105*R*)

Table 2 shows the specification of each grid. Most of the grid points are concentrated in inner-background grid, which captures the trace of tip vortex during several rotations. The number of grid points in span-wise direction of blade grid is considerably increased to model the active flap. The grid spacing of inner background grid corresponds to 0.1c, where c is the blade chord length.

3.2 Aerodynamics & Acoustics

A three-dimensional unsteady flow solver[22] for the Euler equation is used to analyze the aerodynamics of active flap. In the calculation of blade grid, inviscid flux vectors are separated using Roe's flux difference splitting (FDS) algorithm, where flux difference across a cell interface is divided into the components associated with each characteristic wave with second-order accuracy using a TVD scheme. TVD scheme is known to be good in capturing shock wave without adding artificial dissipation. Since Roe's approximate Riemann solver does not have the consistency with the entropy condition and thus permits physically inadmissible expansion shock, an entropy correction is applied to resolve this inconvenience. For the time integration, first-order Euler backward scheme is used in the conventional delta form and the time accuracy is improved by adding the Newton iteration. A diagonalized ADI method with an upwind flux-split technique is used in the linearized implicit part for the discretized governing equations.

In the calculations of background grids, the flux difference across cell interface is divided using a compact TVD scheme[23]. MUSCL cell interface value is modified to achieve 4th-order high accuracy in the background Cartesian grids. Simple High-resolution Upwind Scheme (SHUS)[24] is employed to obtain numerical flux. SHUS is one of the Advection Upstream Splitting Method (AUSM) type approximate Riemann solvers and has small numerical diffusion. The four stage Runge-Kutta method is used for time integration. The free stream condition is applied for the outer boundary of outer background grid.

Acoustic signal is calculated by an acoustic code[25] using the pressure distribution on blade surface obtained by the CFD code as input data. The acoustic code is based on the Formulation 1[26] of Ffowcs Williams and Hawkings (FW-H) formulation.

3.4 Trim Calculation of MuPAL-ε

Among measured flight conditions, instantaneous values at "steady" condition are selected to avoid BVI noise variation due to unsteady pilot controls and acceleration/deceleration. The periods of measured acoustic data were chosen by applying the constraints for roll rate, pitch rate, and acceleration relative to ground as following.

$$\left|\frac{d\Phi}{dt}\right| < 1\,\mathrm{deg/sec}, \quad \left|\frac{d\Theta}{dt}\right| < 1\,\mathrm{deg/sec}, \quad \left|\frac{dV_g}{dt}\right| < 0.1m/\mathrm{sec}^2$$

From the chosen measured flight conditions, necessary properties such as airspeed, vertical speed, and roll angle are determined. Then a flight simulation code was used to estimate the trim conditions, or the blade motion at measured flight conditions.

The flight simulation code calculates the motion of aircraft by six degree-of-freedom equations of a rigid body. The aerodynamic force acting on the main rotor is estimated using the blade element theory. Aerodynamic coefficients of the fuselage are based on the results of wind tunnel tests by the aircraft manufacturer. Small changes of cyclic and collective pitch angles of the blades are made in iterative calculation to trim force and moment until estimated centrifugal force is balanced to achieve trim conditions in turning flight as shown in Fig.4. As a result blade pitching and flapping angles are decided, and these trim data are used for CFD calculation.

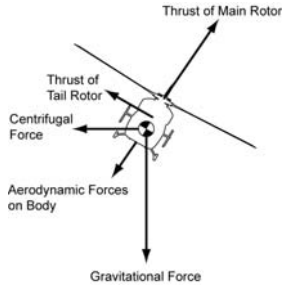

Fig.4: Force balance during turning flight

4. RESULTS AND DISCUSSIONS

4.1 Analysis for Measured Acoustic Data

Figure 5 shows the distribution of maximum noise for descending flight test according to various bank angles. Even there are some variations in magnitude, we can see the distinct tendency of noise increase as the magnitude of bank angle increase for tuning flight. Although wind effect is inevitable in flight test, the aircraft are supposed to fly as

steady as possible in order to compare the measured data with the CFD results. Wind in flight test makes it difficult not only to control the scheduled flight condition but also to analyze the measured acoustic data.

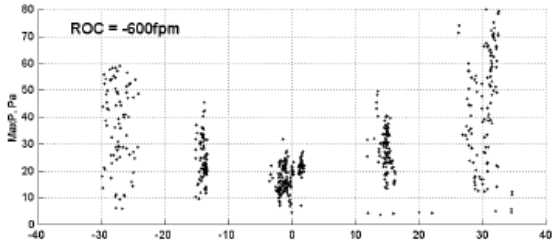

Fig. 5: distribution of maximum noise

Maintaining airspeed constant during turning flight in wind resulted in change of ground speed, and this acceleration/deceleration causes the change of TPP angle of attack. Also the change of miss-distance causes the strength of BVI noise. It is shown that the wind speed varied between 17-29 knots due to both temporal and spatial variation, and maintaining airspeed constant resulted in then change of ground speed. Since the change of ground speed or acceleration/deceleration causes the change of the main rotor tip-path-plane angle, the measured BVI noise varies during measurement. The chosen cases for comparison with CFD computation are to avoid BVI noise variation due to unsteady pilot controls and acceleration/deceleration by the wind. Furthermore, the periods with small temporal variation of flight path angle (around 1deg/sec) were chosen. Figure 6 shows the measured raw and filtered waveforms during one rotor revolution in straight descent and descending turn. It is shown that maximum sound pressure in descending turn is 52.4Pa, and it is twice the maximum pressure of 26.5Pa in straight descending.

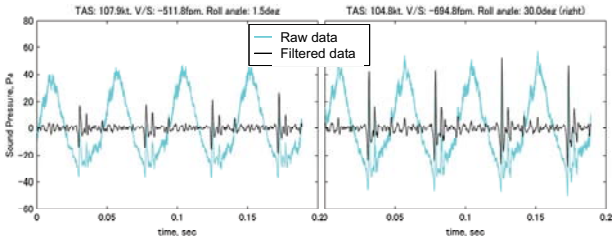

(a) Straight descent (b) Descending turn

Fig. 6: Measured sound pressure for straight descent flight and descending turn flight

4.2 Analysis on Calculated Aerodynamic & Acoustic Data

The CFD code described in Sec.3 is used to analyze the flight test in Sec. 2. The instantaneous surface pressure at 4 view points for different flight condition can be shown in Fig. 16. The fight in descending turn keeps 30 degrees bank angle, which is represented and 30 degree roll of fuselage and rotor. Figure 7 shows vorticity iso-surface at 3 view points and at one intersectional plane. Iso-surface of vorticity is drawn at perspective view (left top), top view (right top), and side view (left bottom). The traces of tip vortex can be examined by vorticity analysis along the intersectional plane (right bottom).

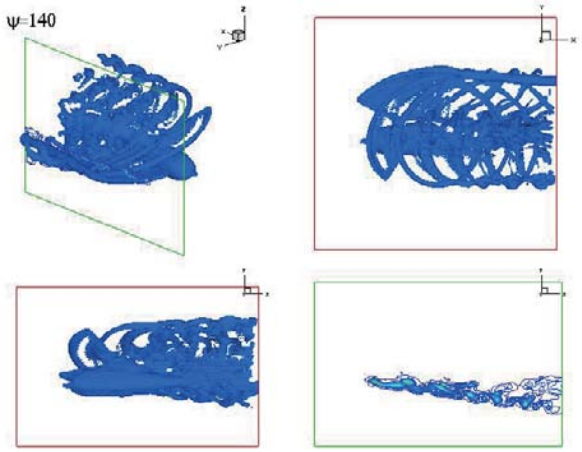

(a) Straight Descent

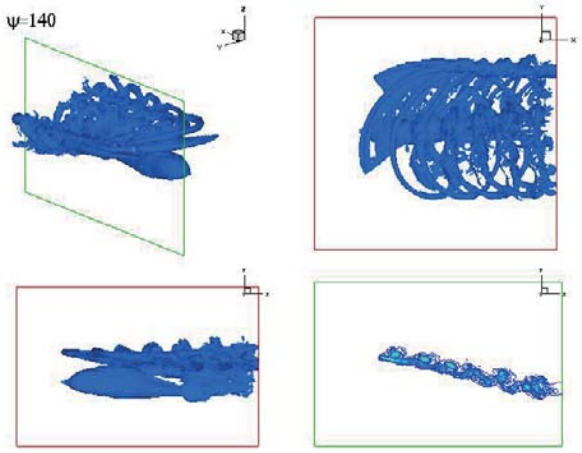

(b) Descending turn

Fig. 7: Vorticity iso-surface

For the better understanding of the phenomena, unsteady pressure histories at surface point of 3% chord and 90% span are shown in Fig. 8. The changes of surface pressure are converted to the change in BVI noise by noise analysis using aero-acoustic solver at the Microphone position or at a far-field position. The overall patterns of CnM2 curves are almost same, which is reasonable from the fact that the flight conditions are not so much different between straight descent flight and descending turn flight except the bank angle. When zooming the azimuth angle range from 20 to 80 degrees where the mainly strong BVI noise occurs, the pressure variation of descending turn flight shows stiffer gradient than that of straight turn flight. This implies the BVI noise of descending turn flight be larger than straight turn flight.

Fig 9 shows the comparison of calculated sound pressures for straight descent flight and descending turn flight at one observer position which is 100*R* in front of rotor disk. As expected from the CnM2 analysis, larger BVI noise for the descending turn flight is captured than that of straight descent flight. This is the same tendency of measured sound data, which implies that CFD simulation successfully reproduces the tendency of increasing BVI noise due to the turning maneuver at least for the present flight conditions.

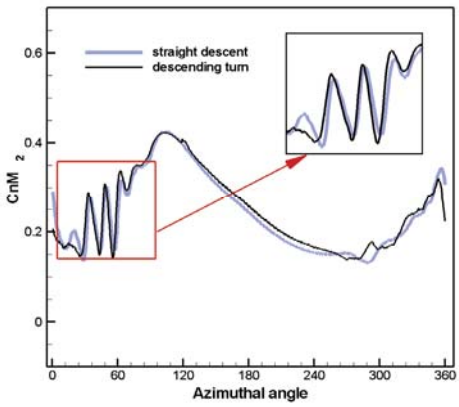

Fig. 8: Unsteady pressure history at surface point of 3% chord and 90% span

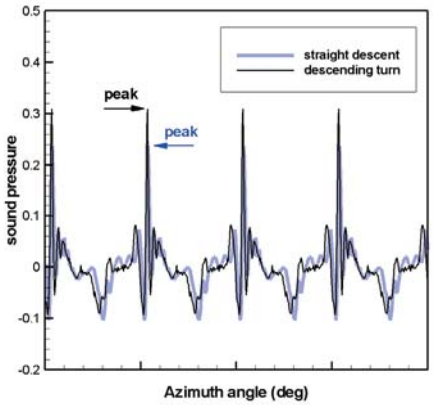

Fig.9: Sound pressure at observer at 100*R* front position

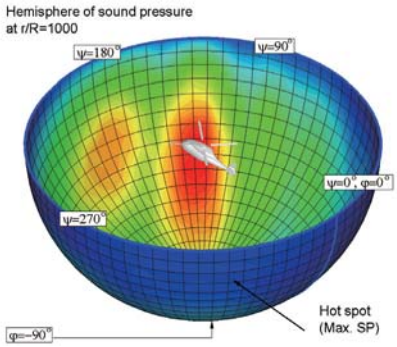

Fig.10: Directivity of BVI noise in hemisphere of sound pressure at *r/R*=100

One of the convenient way to understand the noise directivity in helicopter is using a hemispherical surface of which center is located at the origin of main-rotor (or helicopter) as shown in Fig. 10. A point on the hemispherical surface is specified by the radius, r, the azimuth angle, ψ, and the elevation angle, φ. The azimuth angle follows the count-clockwise main-rotor rotation when viewed from above. Elevation angle is defined as a negative value downward from the tip-path plane of the main-rotor. The contour values on the hemispherical surface represent the peak sound pressure which is radiated from the main-rotor during one revolution at the distance of *r/R*=1000. The peak sound pressure is obtained from the maximum sound pressure in one revolution at each point of hemisphere in Fig. 10.

To make the comparison easier, 2D planar views of hemisphere are drawn in Fig. 11 by spreading hemisphere in plane. The difference in maximum peak sound pressure positions and magnitude of sound pressure are listed in Table 3. Comparing peak noise level contours, the peak positions slightly moved from (ψ=135°, φ=-40°) to (ψ=135°, φ=-40°) by the effect of bank angle during turn. Also the peak noise increases in turning flight. The reason of noise increase can be thought to come from the change of tip path plane angle which gives rise to the change of miss-distance. Vortex bundling in advancing side can be another reason, but confident evidence could not be found for the present flight condition of steady turn. It needs more discussion and analysis of computation results to find out the mechanism of BVI noise increase during turning flight. At least, from this noise analysis, we can confirm the directivity and maximum peak of BVI noise is slightly changed according to the flight conditions.

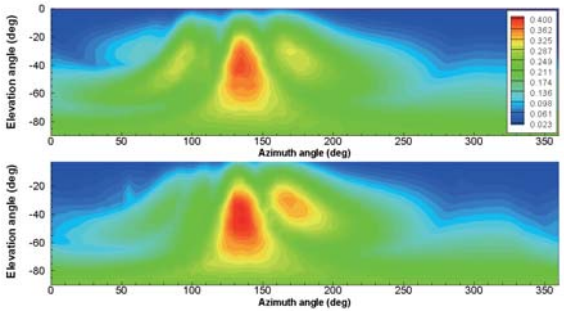

Fig.11: Peak noise contours for BVI

Table 3: Peak noise positions and value

case	ψ	φ	SP(Pa)
Straight descent	135˚	-40˚	0.39
Descending turn	135˚	-45˚	0.45

5. SUMMARY

From flight conditions of flight tests by MuPAL-ε research helicopter, two cases, a straight descent and a descending turn, are chosen to compare the noise pattern with CFD computation and to understand the BVI noise characteristics during coordinate turns. As the results, CFD simulation successfully reproduces the tendency of increasing BVI noise due to the turning maneuver at least for the present flight conditions.

For the full understanding and analysis on the noise characteristics of the turning flight, more flight test cases should be compared with CFD computation results of MuPAL-ε research helicopter.

Although the test cases are chosen to avoid the wind effect as much as possible, the measured data include considerable wind effect. In order to enable “steady” turn with minimum wind effect, new flight tests were conducted around sunrise in

middle of April 2007. Analysis on the acoustic and flight data for further comparison with CFD is ongoing at present, which can help us understand the characteristics of BVI noise in turning flight, as well as reveal the effect of wind on BVI noise.

ACKNOWLEDGEMENT

Authors would like to thank Dr. Ben Wel-C. Sim of NASA Ames Research Center for his valuable advices during discussion on the analysis of measured flight data.

REFERENCES

1. Boxwell, D. A. and Schmitz, F. H., Full-Scale Measurements of Blade-Vortex Interaction Noise, Journal of the American Helicopter Society, Vol.27, (4), Oct, 1982, pp.11-27.
2. Schmitz, F., and Yu, Y., Helicopter Inpulsive Noise: Theoretical and Experimental Status, NASA TM-84390, 1983.
3. Brooks, T., Marcolini, M., and Pope, D., Main Rotor Broadband Noise Study in the DNW, Journal of the American Helicopter Society, Vol.34, No.2, pp.3-12, 1989.
4. Schmitz, F., and Sim, B., Radiation and Directionality Characteristics of Helicoter Blade-Vortex Interation Noise, Journal of the American Helicopter Society, 2003.
5. Brentner, K. S., and Jones, H. E., Noise Prediction For Maneuvering Rotorcraft, AIAA 2000-2031, 2000.
6. Brentner, K. S., Perea, G., Bres, G. A., and Jones, H. E., Toward a Better Understanding of Maneuvering Rotorcraft Noise, AHS 58th Annual Forum, Montreal, Canada, June 2002.
7. Ananthan, S., and Leishman, J. G., Predictions of Transient Rotor Wake Aerodynamics in Response to Time-dependent Blade Pitch Inputs, AHS 59th Annual Forum, Phoenix, AZ, May 2003.
8. Chen, H., Brentner, K. S., Ananthan, S., and Leishman, J. G., A Computational Study of Helicopter Rotor Wakes and Noise Generated During Transient Maneuver, AHS 61st Annual Forum, Grapevine, TX, May 2005.
9. Chen, H., Brentner, K. S., Shirey, J. S., and Horn, J. F., A Study of the Aerodynamics and Acoustics of Super-BVI, AHS 62nd Annual Forum, Pheonix, Arizona, May 2006.
10. Munsky, B., Gandhi, F., and Tauszig, L., An Analysis of Helicoter Blade-Vortex Interaction Noise with Flight Path or Attitude Modification, AHS 58th Annual Forum, Montreal, Canada, June 2002.
11. Perez, G., Costes, M., A New Aerodynamic & Acoustic Computation Chain for BVI Noise Prediction in Unsteady Flight Conditions, AHS 60th Annual Forum, Baltimore, USA, June 2004.
12. Yang, C., Aoyama, T., and Saito, S., Numerical Analysis of Blade-Vortex Interaction Noise in Maneuvering Flight Using Moving Overlapped Grid Method, AHS 62nd Annual Forum, Pheonix, Arizona, May 2006.
13. Okuno, Y. and Matayoshi, N., "Development of a New Research Helicopter MuPAL-ε," 57th AHS Annual Forum, 2001.
14. Ochi, A., Aoyama, T., Saito, S., Shima, E., and Yamakawa, E., BVI Noise Predictions by Moving Overlapped Grid Method, AHS 55th Annual Forum, Montreal, Canada, May 1999.
15. Yang, C., Aoyama, T., and Saito, S., Numerical Study on BVI Noise Reduction Using Active Flap Control, 31st ERF, No. 24, Florence, Italy, September, 2005.
16. Aoyama, T., Yang, C., and Saito, S., Numerical Analysis of Active Flap for Noise Reduction Using Moving Overlapped Grid Method, AHS 61st Annual Forum, Grapevine, TX, June, 2005.
17. Aoyama, T., Yang, C., and Saito, S., Numerical Analysis of Interaction Noise Between Main Rotor and Tail Rotor of Helicopter, 24th International Congress of the Aeronautical Science (ICAS), Yokohama, Japan, 29 Aug.-3 Sep.,2004.
18. Nojima, T., Funabiki, K., and Iijima, T., Flight Demonstration of a New Operational Concept Using TDMA Data Link System , 24th Congress of International Council of the Aeronautical Sciences, 2004.
19. Ishii, H., Gomi, H., and Okuno, Y., Helicopter Flight Tests for BVI Noise Measurement Using an Onboard External Microphone, AIAA 2005-6119, Atmospheric Flight Mechanics Conference and Exhibit, 2005.
20. Chen, R. T. N., Hindson, W. S., and Mueller, A. W., "Acoustic Flight Tests of Rotorcraft Noise-Abatement Approaches Using Local Differential GPS Guidance," NASA TM-110370, 1995.
21. Kitaplioglu, C., Betzina, M., and Johnson, W., "Blade-Vortex Interaction Noise of an Isolated Full-scale XV-15 Tilt-rotor," American Helicopter Society 56th Annual Forum, 2000
22. Aoyama, T., et al., Unsteady Calculation for Flowfield of Helicopter Rotor with Various Tip Shapes, 18th European Rotorcraft Forum, Paper No.B03, Avignon, France, September 1992.
23. Yamamoto, S. and Daiguji, H., Higher-Order-Accurate Upwind Schemes for Solving the Compressible Euler and Navier-Stokes Equations, J. of Computers & Fluids, 22, pp.259-270, 1993.
24. Shima, E. and Jounouchi, T., Role of CFD in Aeronautical Engineering (No.14) - AUSM type Upwind Schemes -, NAL SP-34, 1999, pp. 7-12.
25. Nakamura, Y., and Azuma, A., "Rotational Noise of Helicopter Rotors," Vertica, vol. 3, No. 3/4, pp.293-316, 1979.
26. Farassat, F., Theory of noise generation from moving bodies with an application to helicopter rotors, NASA TR R 451, 1975.